

# Quantum phases of strongly interacting Rydberg atoms in triangular lattices

Jing Qian, Lu Zhou and Weiping Zhang

*Quantum Institute for Light and Atoms, Department of Physics,  
East China Normal University, Shanghai 200062, People's Republic of China*

We present a theoretical study on the system of laser-driven strongly interacting Rydberg atoms trapped in a two-dimensional triangular lattice, in which the dipole-dipole interactions between Rydberg states result in exotic quantum phases. By using the mean-field theory, we investigate the steady state solutions and analyze their dynamical stabilities. We find that in the strong-interaction limit, the dynamics of the system is chaotic and exhibits random oscillations under appropriate laser detunings. Lyapunov exponent criterion is introduced to confirm the existence of this chaotic behavior. In addition, we present a full quantum calculation based on a six-atom model, and find that the system exhibits some bi-antiferromagnetic properties in every triangular cell when the one-photon detuning is exactly resonant or blue-shifted.

*Introduction:* Ultracold atomic gases loaded in an optical lattice can provide a clean and highly controllable platform to study various phenomena in condensed matter physics [1, 2]. Due to the remarkable control of physical parameters, such as the hopping rate or the on-site interaction strength, one can not only simulate the quantum many-body physics of solid-state systems, but also explore exotic quantum phases in the parameter regimes inaccessible to real solid-state materials. Recently, two new developments have taken place in this area. Firstly, experimental techniques for the preparation of dipolar quantum gas have been rapidly advancing over the last few years. This has been demonstrated by the realization of Bose-Einstein condensation of chromium atoms which have large magnetic dipole moments [3] and by the creation of quantum degenerate states of Rydberg atoms which have very large induced electric dipole moments [4, 5]. Secondly, optical lattices with non-cubic geometrical configurations have been introduced in this area [6, 7]. Typical examples include the experimental observation of the superfluid to Mott insulator phase transition of rubidium atoms in triangular optical lattices [8], and quantum simulation for triangular magnetism with the motional degrees of freedom of atoms [9].

Due to its long-range nature, the dipolar interaction between atoms should lead to novel kinds of quantum phases in the strongly interacting regime [10]. A typical example is bistable or non-equilibrium phase caused by dipole blockade effect in Rydberg atom gas [11]. Moreover, the dipolar interaction coupled with the geometry of the triangular lattice can produce more interesting effect named geometrical frustration [12–14]. A rich variety of possible quantum phases arise from it, such as spin glass [15], spin liquid [16], and spin ice [17–19]. They attract a large amount of interests in solid state physics owing to their intrinsic link to high temperature superconductivity. Stimulated by these researches, we focus on a system of ultracold Rydberg atoms loaded into a two-dimensional (2D) triangular optical lattice as shown in Fig. 1(a). The recent new progress in experiments could make it an ideal system to investigate the effect of geometrical frustration in the near future.

In our study, with the mean-field treatment, we inves-

tigate the steady state phases of Rydberg atoms under strong dipole-dipole interactions (DDIs) [20]. The dipole blockade effect results in a suppression of Rydberg excitation for atoms in the nearest-neighbor (NN) lattice sites [21], which may give rise to a typical antiferromagnetic phase as predicted in Ref. [11]. However, the triangular geometry adds frustration effect into the scheme which results in very different quantum phases from the square lattice case [22]. Except the uniform and nonuniform phases that are stable when the laser detuning and DDIs are dominated, respectively, bistable, oscillatory, and even chaotic phases are predicted in this system. In addition, we also perform a full quantum numerical simulation on a six-atom 2D model in a similar parameter region to compare with the mean-field results.

*Mean-field model:* We consider a 2D triangular lattice with exactly one two-level atom per site. We assume that the lattice depth is deep enough so the center-of-mass motion of the atoms can be safely neglected. An off-resonant laser beam uniformly illuminates the atoms, driving the transition between the atomic ground state  $|g\rangle$  and the Rydberg state  $|r\rangle$ . In the interaction picture, the total Hamiltonian of the system reads  $\mathcal{H} = \sum_j \mathcal{H}_j + \mathcal{V} \sum_{k \neq j} |r\rangle \langle r|_j \otimes |r\rangle \langle r|_k$ , with  $\mathcal{H}_j$  describing the atom at the  $j$ -th lattice site and its coupling to the laser field,

$$\mathcal{H}_j = -\Delta |r\rangle \langle r|_j + \frac{\Omega}{2} \left( |r\rangle \langle g|_j + |g\rangle \langle r|_j \right), \quad (1)$$

where  $\Delta$  is the detuning between the laser frequency and atomic transition frequency and  $\Omega$  is the single-photon Rabi frequency. The second term in total Hamiltonian  $\mathcal{H}$  is for the DDIs between Rydberg states of atoms. Since its strength decreases rapidly as the inverse of  $(a|j-k|)^6$  with  $a|j-k|$  the distance between lattice sites  $j, k$  and  $a$  the nearest distance, we truncate the summation to the NN sites [23]. If we treat the two-level atom as a spin-1/2 particle, the total Hamiltonian is formally equivalent to an Ising model with exchange energy  $\mathcal{V}$  and transverse external field of strength  $\Omega/2$  [24].

In order to obtain the quantum phases of the system, one should solve the steady state solutions of the master equation:

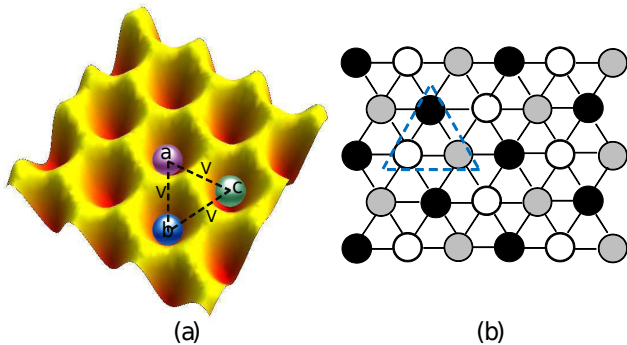


FIG. 1: (Color online) (a) Schematic diagram of the smallest triangular cell of three atoms (a, b and c) trapped in a two-dimensional triangular lattice. The nearest-neighbor interatomic interaction is denoted by  $\mathcal{V}$ . (b) This two-dimensional lattice is composed of three interpenetrating sublattices marked in black, white and gray colors, respectively. The dashed blue frame indicates the smallest triangular unit.

$$\dot{\rho} = -i[\mathcal{H}, \rho] + \mathcal{L}[\rho], \quad (2)$$

where the spontaneous emission process from the Rydberg state with decay rate  $\gamma$  is described by the Lindblad operator  $\mathcal{L}[\rho]$ ,

$$\mathcal{L}[\rho] = \gamma |g\rangle \langle r|_j \rho |r\rangle \langle g|_j - \frac{\gamma}{2} \left\{ |r\rangle \langle r|_j, \rho \right\}. \quad (3)$$

For the 2D and large-number atomic system considered here, the mean-field approximation (MFA) is a good treatment to simplify the master equation [25]. Under the MFA, we can neglect the intersite quantum correlations and factorize the density matrix each site. Then the master equation (2) is reduced to the nonlinear coupling equations,

$$\dot{\rho}_{j,rr} = \Omega \text{Im}(\rho_{j,gr}) - \rho_{j,rr}, \quad (4a)$$

$$\dot{\rho}_{j,gr} = -i\Delta_{j,eff}\rho_{j,gr} - \frac{1}{2}\rho_{j,gr} + i\frac{\Omega}{2}(1 - 2\rho_{j,rr}) \quad (4b)$$

where we have introduced the single-site density matrix elements  $\rho_{j,rr}$  and  $\rho_{j,gr}$  to describe the  $j$ th atom's Rydberg state population and atomic coherence, respectively. The effective detuning for the  $j$ th atom,  $\Delta_{j,eff} = \Delta - \mathcal{V} \sum_{k \neq j} \rho_{k,rr}$  is renormalized by the excitation probabilities of its neighbors. In arriving at Eqs. (4), the frequency is scaled with  $\gamma$  and time with  $1/\gamma$ .

In order to include all the NN interactions and the effect of the geometrical frustration, we factorize the triangular lattice into three interpenetrating sublattices that are labeled by  $j = 1$  (black), 2 (white) and 3 (gray) as shown in Fig.1(b). In that way, only NN interactions between Rydberg atoms from different sublattices are considered, hence the steady state solutions  $\rho_{j,rr}^s$  to Eqs. (4) are governed by the following equations:

$$\rho_{j,rr}^s = \frac{\Omega^2}{4(\Delta_{j,eff}^s)^2 + 1 + 2\Omega^2}, \quad (j = 1, 2, 3) \quad (5)$$

with  $\Delta_{j,eff}^s = \Delta - \mathcal{V} \sum_k \rho_{k,rr}^s$ ,  $k = 1, 2, 3$  and  $k \neq j$ . The superscript  $s$  stands for the stationary solution. In general, the quantum phases decided by  $\rho_{j,rr}^s$  can be classified into uniform and nonuniform phases. The uniform phase (UNI) can also be called ferromagnetic phase, because it corresponds to a spatially homogeneous Rydberg excitation probability, i.e.  $\rho_{1,rr}^s = \rho_{2,rr}^s = \rho_{3,rr}^s$ . However, due to the triangular geometry, the nonuniform phase has several different types, they are:

a) Bi-antiferromagnetic phase (BAF): BAF phase corresponds to the case that atoms in two of the three sublattices have the same Rydberg excitation probability, e.g.  $\rho_{1,rr}^s = \rho_{2,rr}^s \neq \rho_{3,rr}^s$ . This is similar to the "Y" state in classical triangular Heisenberg antiferromagnet [26]. Physically, this originates from the geometric frustration by which all the neighboring "spins" on the triangles can not align antiparallel to each other at the same time. The ground state is composed of two spins of one kind and one of another in each triangle. When  $\rho_{1,rr}^s = \rho_{2,rr}^s < \rho_{3,rr}^s$ , we define it as BAF1; when  $\rho_{1,rr}^s = \rho_{2,rr}^s > \rho_{3,rr}^s$ , we define it as BAF2.

b) Tri-antiferromagnetic phase (TAF): TAF phase corresponds to exact nonuniform steady-state solutions which requires  $\rho_{1,rr}^s \neq \rho_{2,rr}^s \neq \rho_{3,rr}^s$ . This phase is a distorted version of the "120-degree state" in Heisenberg antiferromagnet [26].

*Phase diagram:* In Fig. 2, we show the steady state solutions  $\rho_{j,rr}^s$  ( $j=1,2,3$ ) and its stability with the tunable one-photon detunings  $\Delta$  at two different cases: (a) the weak interaction case with  $\mathcal{V}/\Omega = 5$  and (b) the strong interaction case with  $\mathcal{V}/\Omega = 20$ . A similar and detailed demonstration for the phases and their stabilities based on a cubic lattice with three-level atoms has been presented in our recent work [22]. Here, we mainly focus on the new findings for this triangular configuration.

In the weak interaction case, we find the system allows the existence of rich stable phases that contains UNI, BAF1, BAF2 and TAF phases. By changing  $\Delta$  from negative, there are two subcritical pitchfork bifurcations: one is at  $\Delta_{c1} = 0.90$  in which the system undergoes a phase transition from UNI phase to BAF1 phase; the other is at  $\Delta_{c2} = 2.76$  in which the system transits back to UNI phase from BAF2 phase. The subcritical pitchfork bifurcation means these phase transitions are discontinuous, that is contrast to the case for square lattice [11]. In addition, the triangular geometry also enables a stable TAF phase at the region  $\Delta \in [1.70, 1.79]$ , which plays a role of transitional phase between BAF1 and BAF2 phases. Moreover, bistability takes place between two different UNI phases, UNI and BAF1 phases and UNI and BAF2 phases, which is a typical nonlinear effect due to the Rydberg interactions.

The impact of nonlinear Rydberg couplings combined

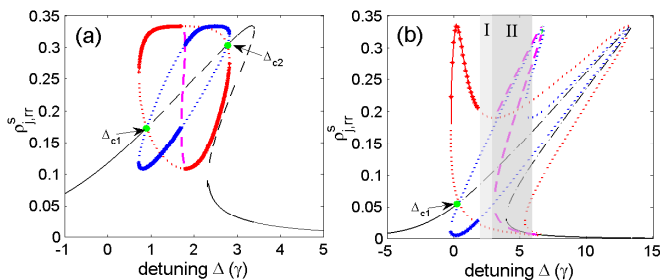


FIG. 2: (Color online) Steady-state solutions  $\rho_{j,rr}^s$  ( $j = 1, 2, 3$ ) versus detuning  $\Delta$ . Stable and unstable uniform solutions are denoted by solid black and dashed black lines. TAF solutions are denoted by dashed magenta lines. Stable and unstable BAF solutions are denoted by thick solid lines with cross symbols and thick dotted lines. The two same stationary solutions in BAF phase are marked in blue color and the third one is marked in red color. (a) The weak interaction case with  $\mathcal{V} = 5$ ; (b) The strong interaction case with  $\mathcal{V} = 20$ . Light shadow regime I corresponds to the dynamical oscillatory solutions, and dark shadow regime II to the chaotic behaviour. Other parameter is  $\Omega = 1.0$ .  $\gamma$  is the frequency unit.

with triangular geometry becomes more prominent when turning to the strong interaction case. Different from the weak interaction case, now the phase diagram [see Fig.2(b)] shows a clear three-peak character. From left to right, the first peak located at  $\Delta \approx 0$  corresponds to the single-atom resonance which requires e.g.  $\Delta_{3,eff}^s = 0$ ,  $\Delta_{(1,2),eff}^s \neq 0$ ; the second at  $\Delta = \mathcal{V}\Omega^2 / (1 + 2\Omega^2)$  corresponds to the double-atom resonance which requires e.g.  $\Delta_{(1,2),eff}^s = 0$ ,  $\Delta_{3,eff}^s \neq 0$ ; the third at  $\Delta = 2\mathcal{V}\Omega^2 / (1 + 2\Omega^2)$  corresponds to the three-atom resonance which requires  $\Delta_{(1,2,3),eff}^s = 0$ . The stability of these stationary solutions are numerically checked and unstable solutions are labeled by dashed and dotted lines. Clearly, at single-atom resonance the stationary solutions are stable, which means that the Rydberg blockade effect is very efficient [27]. When  $\Delta$  increases to satisfy two multi-atom resonance conditions, the stationary solutions are both unstable, indicating inefficient Rydberg antiblockade effect [28, 29]. By solving the resonances, we also note that  $\max[\rho_{j,rr}^s] = \Omega^2 / (2\Omega^2 + 1) \rightarrow 1/2$  if  $\Omega \rightarrow +\infty$ , which is consistent with the steady state solution of the optical Bloch equations for an isolated two-level atom [30]. In our calculations,  $\max[\rho_{j,rr}^s] = 1/3$ .

Besides, different from the weak interaction case, there are some parameter regions without any stable phases. As  $\Delta$  crosses the critical point  $\Delta_{c1}$  and increases to the values in shadow region I, the Rydberg state populations start to oscillate periodically in time [see Fig.3(c)], until entering shadow regime II where the population evolutions become irregular and complex [see Fig.3(d)]. We will show below that they indicate the emergence of chaos. When  $\Delta$  is even large blue-shifted, the system turns back to uniform and low-excitation. To demonstrate the existence of BAF1 phase (not BAF2 or TAF),

we introduce a simple model with three atoms in which two of them interact strongly, forming a typical two-atom Rydberg blockade model [31]. As a third atom is brought closer towards this atomic pair, it feels strong DDIs induced by the highly-excited pair, and the other ground state atom does not affect the third one. As a result, it is only possible to obtain stable BAF1 phase in the strong interaction case.

It is worthwhile to state that the model we considered in this work is an open system. The presence of driving and dissipation leads to remarkable nonequilibrium phenomena in our model, such as periodic oscillation of Rydberg excitation and bistability between different phases [10]. Moreover, except for the support for various frustration phases, e.g. BAF and TAF phases, the triangular geometry also plays a key role in generating chaos in this open system, which is an important behavior in nonequilibrium statistics and is absent in square lattice case.

*Lyapunov exponent and Chaos:* The motions in the chaotic environment could show very sensitive dependence to the initial conditions. This means two trajectories starting very close to each other will rapidly diverge, and can have totally different futures. To measure this sensitivity and to verify that chaos is not a just long-period oscillation, we introduce a parameter named "Lyapunov exponent" [32]. The presence of at least one positive Lyapunov exponent value can be regarded as the signature of chaos. For that, we introduce the definition of "maximal Lyapunov exponent" (MLE):

$$\lambda_{\max} = \lim_{t \rightarrow \infty} \lim_{\delta Z_0 \rightarrow 0} \frac{1}{t} \ln \left| \frac{\delta Z(t)}{\delta Z_0} \right| \quad (6)$$

which describes two trajectories with initial small separation  $\delta Z_0$  diverge as a function of  $\delta Z(t)$  with time  $t$ .

In Fig. 3(a) we plot the MLE values of  $\rho_{1,rr}$  in the parameter space of  $(\Delta, \mathcal{V})$  by numerically solving Eqs. (4). Most of areas in darkgray correspond to stable phases in which MLE is strictly negative. Such stable phases include UNI, BAF1, BAF2 and TAF for weak interactions and UNI, BAF1 for strong interactions that is consistent with our former results. The positive MLE values corresponding to the chaos only emerge in a small white area, where the interaction strength  $\mathcal{V}$  is larger than the single-atom energy represented by the negative detuning  $-\Delta$  and Rabi frequency  $\Omega$ . Besides, there is also a lightgray area around the chaotic area, whose MLE values are very close to zero. The existence of this intermediate area is because when the system has a chaotic tendency, it always first starts to oscillate quasi-periodically.

Figure 3(b)-(d) show the Rydberg-state population evolutions  $\rho_{j,rr}^t$  ( $j=1,2,3$ ) for three sublattices in the BAF1 phase, oscillatory phase and chaotic regimes, respectively. Fig. 3(b) clearly shows that the system is stable at BAF1 phase in which two atoms within a single triangular sublattice exhibit lower excitation probabilities than the third one. This is due to the Rydberg blockade effect. By increasing  $\Delta$  to 2.0 (in the lightgray regime of

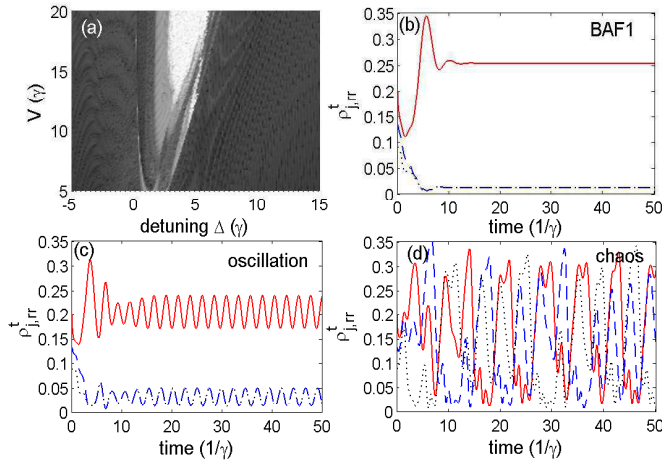


FIG. 3: (Color online) (a) MLE values in  $(\Delta, \mathcal{V})$  space with initial Rydberg populations  $\rho_{1,rr}^{t=0} = 0.2$ ,  $\rho_{2,rr}^{t=0} = 0.15$ ,  $\rho_{3,rr}^{t=0} = 0.1$  and a small separation  $\delta\rho_{1,rr}^{t=0} = 10^{-6}$ . The positive, near-zero and negative values are respectively labeled by white, lightgray and darkgray colors, corresponding to chaos, oscillatory phase and stable phase; (b)-(d) show typical Rydberg population dynamics  $\rho_{i,rr}^t$  (solid),  $\rho_{2,rr}^t$  (dashed),  $\rho_{3,rr}^t$  (dotted) of BAF1 phase ( $\Delta = 1.0$ ), oscillatory phase ( $\Delta = 2.0$ ) and chaotic behavior ( $\Delta = 5.0$ ) with  $\mathcal{V} = 20$ . Other parameters are  $\Omega = 1$ ,  $\gamma t = 50$ .

(a), the system enters into the oscillatory phase with the Rydberg populations periodically oscillating surround its original fixed points [see Fig.3(c)]. For a larger detuning [Fig.3(d)], the system undergoes a transition to the chaotic motion where the periodic oscillations become random and irregular. We note that there are various ways for the dynamics of a classical system trends to be chaotic, such as period-doubling oscillation [33], intermittent chaos [34], and quasi-periodic oscillation [35, 36] which is the approach for the present system.

*Full quantum simulation:* To complement the above analysis with MFA, we present a full quantum simulation for a six-atom 2D lattice by solving the original master equation (2). The lattice includes four triangular cells as shown in the inset of Fig. 4(b). Following Ref. [11], we introduce a quantity  $\delta_{\mu\nu} = \langle \sigma_\mu \sigma_\nu \rangle - \langle \sigma_\mu \rangle \langle \sigma_\nu \rangle$  with  $\sigma_\mu = |r\rangle \langle r|_\mu$  and  $\mu (v)$  the atomic indices in each cell. This quantity characterizes the quantum correlations between any two atoms in each triangular cell and intimately related to the properties of this system.

In Figure 4 we compare  $\delta_{\mu\nu}$  for different values of detuning  $\Delta$ . For  $\Delta < 0$  (dashed blue line), we observe the difference between each  $\delta_{\mu\nu}$ s is very small, which indicate the uniform phase obtained in MFA treatment. The small negative value of all  $\delta_{\mu\nu}$ s indicates the anti-correlation between NN atoms due to the fact that the probability of two atoms being excited individually is larger than that they are being excited simultaneously, i.e. Rydberg blockade effect. For  $\Delta = 0$  [Fig. 4(a)], we see that in each triangle [A, B, C, D], two of the three  $\delta_{\mu\nu}$ s are always very close and different from the third

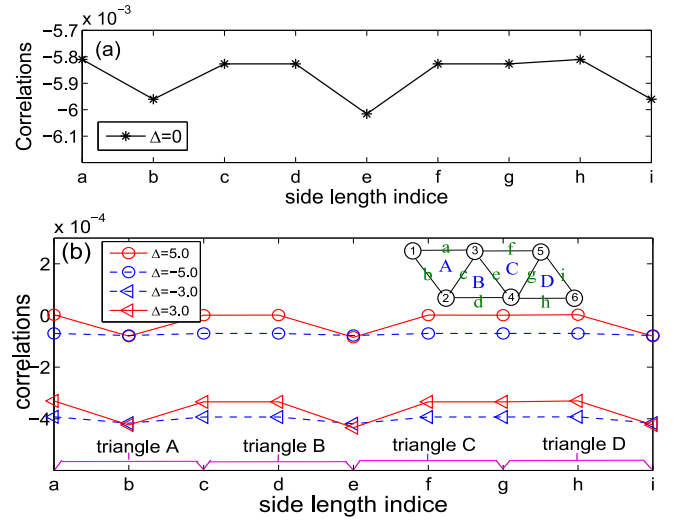


FIG. 4: Quantum calculation solutions of master equation for a six-atom lattice (inset of (b)) with periodic boundary conditions. The correlation quantities  $\delta_{\mu\nu}$  are solved under different detunings.  $a, b, \dots, i$  denote the side length indices in four triangles A, B, C and D. (a)  $\Delta = 0$  (solid stars); (b)  $\Delta = -5$  (solid circles),  $-3$  (dashed triangles),  $3$  (solid triangles),  $5$  (solid circles). Other parameters are the same as in Fig. 3.

one, that confirms the prediction of BAF1 phase with MFA at the same parameters. As  $\Delta$  increases, we find  $\delta_{\mu\nu}$  tends to zero (around  $\Delta = 5$ ) from negative but the difference between  $\delta_{\mu\nu}$ s still remains. That shows a tendency of transition from BAF1 to BAF2 phase. With the further increase of  $\Delta$ ,  $\delta_{\mu\nu}$  become positive, corresponding to BAF2 phase due to the anti-blockade effect (not show in the figure).

In our full quantum calculation, the oscillatory and chaotic phase are not observed. That is because these nonequilibrium phases originates from the nonlinear coupling between the density matrix elements of the NN atoms in MFA equations (4) [see the definition of  $\Delta_{j,eff}$ ] [37]. However, the present quantum model consists of only six atoms, which is obviously far from the effective regime of MFA, so that it can not display the quantum counterparts of these phases. Actually, in order to investigate the corresponding quantum behaviors of a chaotic system, its quasi-probability distribution in phase space should be calculated [38]. This problem will be addressed in our future works.

*Conclusions:* We have investigated quantum phases of strongly interacting Rydberg atoms in a 2D triangular lattice system via MFA. The effect of laser pumping and spontaneous decay are considered. Except the uniform phase, we find that the geometric frustration results in rich phases. By tuning the pump detuning, the system shows BAF phase, TAF phase and even bistable states between these phases. Particularly, in the strong interaction case, the system has no stable phase in some parameter region, in which its dynamics is characterized by

chaotic oscillations. To confirm the existence of chaos, we calculate the maximal Lyapunov exponent and find that it is strictly positive in the chaotic regime. Moreover, we present a full quantum calculation with six atoms to simulate the Rydberg excitation probability and find that it is consistent with the mean-field results.

Our results show that the Rydberg atoms in a triangular optical lattice is a good candidate system to simulate the quantum spin frustration and explore its effect in the nonequilibrium statistics and quantum chaos. In the future works, we will extend our discussion to Rydberg atoms with long-range and anisotropic DDIs, which play the important roles in the generation of spin ice, spin

glass and other unique quantum phases.

This work was supported by the National Basic Research Program of China (973 Program) under Grant No. 2011CB921604, the National Natural Science Foundation of China under Grants Nos. 11104076, 11004057, 11234003, the Specialized Research Fund for the Doctoral Program of Higher Education No. 20110076120004, the "Chen Guang" project from Shanghai Municipal Education Commission and Shanghai Education Development Foundation under Grant No. 10CG24, Shanghai Rising-Star Program under Grant No. 12A1401000 and the Fundamental Research Funds for the Central Universities.

- 
- [1] I. Bloch, *Nat. Phys.* **1** 23 (2005) and reference therein.
- [2] I. Bloch, J. Dalibard and W. Zwerger, *Rev. Mod. Phys.* **80** 885 (2008) and references therein.
- [3] A. Griesmaier, J. Werner, S. Hensler, J. Stuhler and T. Pfau, *Phys. Rev. Letts.* **94** 160401 (2005).
- [4] R. Heidemann, U. Raitzsch, V. Bendkowsky, B. Butscher, R. Löw and T. Pfau, *Phys. Rev. Letts.* **100** 033601 (2008).
- [5] R. Löw, H. Weimer, J. Nipper, J. B. Balewski, B. Butscher, H. P. Büchler and T. Pfau, *J. Phys. B: At. Mol. Opt. Phys.* **45** 113001 (2012) and references therein.
- [6] Y. H. Chen, W. Wu, H. S. Tao and W. M. Liu, *Phys. Rev. A* **82** 043625 (2010).
- [7] A. Dauphin, M. Müller and M. A. M-Delgado, *Phys. Rev. A* **86** 053618 (2012).
- [8] C. Becker, P. S-Panahi, J. Kronjäger, S. Dörscher, K. Bongs and K. Sengstock, *New J. Phys.* **12** 065025 (2010).
- [9] J. Struck, C. Ölschläger, R. L. Targat, P. S-Panahi, A. Eckardt, M. Lewenstein, P. Windpassinger and K. Sengstock, *Science* **333** 996 (2011).
- [10] A. W. Glaetzle, R. Nath, B. Zhao, G. Pupillo, and P. Zoller, *Phys. Rev. A* **86** 043403 (2012).
- [11] T. E. Lee, H. Häfner and M. C. Cross, *Phys. Rev. A* **84** 031402(R) (2011).
- [12] R. Moessner and A. P. Ramirez, *Phys. Today* **59** 24 (2006).
- [13] A. Eckardt, P. Hauke, P. S-Panahi, C. Becker, K. Sengstock and M. Lewenstein, *Europhys. Lett.* **89** 10010 (2010).
- [14] K. Kim, M. S. Chang, S. Korenblit, R. Islam, E. E. Edwards, J. K. Freericks, G. D. Lin, L. M. Duan and C. Monroe, *Nature* **465** 590 (2010).
- [15] S. L. A. de Queiroz, *Phys. Rev. B* **73** 064410 (2006).
- [16] H. Zhou, E. Choi, G. Li, L. Balicas, C. Wiebe, Y. Qiu, J. Copley and J. Gardner, *Phys. Rev. Letts.* **106** 147204 (2011).
- [17] S. T. Bramwell, S. R. Giblin, S. Calder, R. Aldus, D. Prabhakaran and T. Fennell, *Nature* **461** 956 (2009).
- [18] D. J. P. Morris, D. A. Tennant, S. A. Grigera, B. Klemke, C. Castelnovo, R. Moessner, C. Czternasty, M. Meissner, K. C. Rule, J. U. Hoffmann, K. Kiefer, S. Geroscher, D. Slobinsky and R. S. Perry, *Science* **326** 411 (2009).
- [19] T. Fennell, P. P. Deen, A. R. Wildes, K. Schmalzl, D. Prabhakaran, A. T. Boothroyd, R. J. Aldus, D. F. McMorrow, and S. T. Bramwell, *Science* **326** 415 (2009).
- [20] T. F. Gallagher and P. Pillet, *Adv. At., Mol., Opt. Phys.* **56** 161 (2008).
- [21] M. Viteau, M. G. Bason, J. Radogostowicz, N. Malossi, D. Ciampini, O. Morsch and E. Arimondo, *Phys. Rev. Letts.* **107** 060402 (2011).
- [22] J. Qian, G. J. Dong, L. Zhou and W. Zhang, *Phys. Rev. A* **85** 065401 (2012).
- [23] M. Höning, D. Muth, D. Petrosyan and M. Fleischhauer, *Phys. Rev. A* **87** 023401 (2013).
- [24] R. Elliott, P. Pfeuty and C. Wood, *Phys. Rev. Letts.* **25** 443 (1970).
- [25] S. Diehl, A. Tomadin, A. Micheli, R. Fazio and P. Zoller, *Phys. Rev. Letts.* **105** 015702 (2010).
- [26] E. Sela, M. Punk and M. Garst, *Phys. Rev. B* **84** 085434 (2011).
- [27] M. Viteau, P. Huillery, M. G. Bason, N. Malossi, D. Ciampini, O. Morsch, E. Arimondo, D. Comparat and P. Pillet, *Phys. Rev. Letts.* **109** 053002 (2012).
- [28] C. Ates, T. Pohl, T. Pattard, and J. M. Rost, *Phys. Rev. Letts.* **98** 023002 (2007).
- [29] T. Amthor, C. Giese, C. S. Hofmann, M. Weidemüller, *Phys. Rev. Letts.* **104** 013001 (2010).
- [30] P. Meystre, *Atom Optics*. Springer (2001).
- [31] D. Comparat and P. Pillet, *J. Opt. Soc. Am. B* **27** A208(2010).
- [32] M. Cencini, F. Cecconi and A. Vulpiani, *Chaos: From Simple Models to Complex Systems*. World Scientific Publishing Company (2009).
- [33] D. Krefting, P. Kaira and H. H. Rotermund, *Phys. Rev. Letts.* **102** 178301 (2009).
- [34] E. Shlizerman and V. Rom-Kedar, *Phys. Rev. Letts.* **102** 033901 (2009).
- [35] D. Rand, S. Ostlund, J. Sethna and E. D. Siggia, *Phys. Rev. Letts.* **49** 132 (1982).
- [36] K. Zhang, W. Chen, M. Bhattacharya and P. Meystre, *Phys. Rev. A* **81** 013802 (2010).
- [37] S. H. Strogatz, *Nonlinear Dynamics and Chaos*. Perseus Books, Cambridge (1994).
- [38] S. A. Gardiner, J. I. Cirac and P. Zoller, *Phys. Rev. Letts.* **79** 4790 (1997).